Int. J. Electrochem. Sci., 15 **(2020)** 6663 – 6681, doi: 10.20964/2020.07.51

International Journal of
ELECTROCHEMICAL
SCIENCE
www.electrochemsci.org

Study on the Flow Field Characteristics of a New Type of Plug Flow Electrochemical Reactor with a Mesh Plate Electrode

Jia Sheng Li, YingWu Yao, XiaoPing Shi, Jinliang Tao, Feng Wei[*]

School of Chemical Engineering and Technology, Hebei University of Technology, Tianjin 300130, China
[*]E-mail: weifeng@hebut.edu.cn

Received: 9 March 2020 / *Accepted:* 28 April 2020 / *Published:* 10 June 2020

In this paper, a flow field test of a plug flow electrochemical reactor with a mesh plate electrode was carried out by particle image velocimetry (PIV) technology. The internal axial velocity field and the electrode plate surface velocity fields under the simulated conditions of the reactor were analyzed under different flow rates and different plate layouts. The influencing factors of the internal flow field distribution of the reactor were investigated. A numerical fitting of unknown resistance parameters in the reactor was carried out. The experimental results showed that the internal flow field of the reactor was mainly affected by the axial flow of the liquid phase and the escape of the bubble group on the surface of the plates. At higher flow velocities, the energy loss between the reactor electrodes was mainly attributable to the energy loss caused by the mesh plate electrodes. The special geometry and mesh structure of the plate surface had a horizontal guiding effect on the axial flow of the liquid phase.

Keywords: plug flow electrochemical reactor, particle image velocimetry, mesh plate electrode, flow field, gas-liquid two-phase flow

1. INTRODUCTION

In today's society, environmental pollution is worsening. Electrocatalytic oxidation is an effective treatment for wastewater [1-5]. The structure of an electrocatalytic oxidation reactor has a strong influence on the progress of the electrocatalytic oxidation process[6-8]. The hydrodynamics of parallel plate electrochemical reactors have been studied. The results of López-García [9] indicated that the plug flow dominates between the plates. Colli A N[10] found that the axial dispersion coefficient increases linearly with the volumetric flow rate, and an increase in the flow rate is beneficial to mass transfer. Rodríguez G[11] found that the Reynolds number suitable for electrochemical reactor applications is 2200 and proposed CFD as a good method to evaluate the performance of electrochemical reactors. For the structural design of electrochemical reactors, Walsh F C [12] illustrated different electrode formats

and reactor designs. The turbulence intensity can be easily enhanced by including 3-dimensional electrodes, structured electrode surfaces and bipolar electrical connections. The plug flow electrochemical reactor (PFER) is widely used. Bisang J M [13] presented an analysis of the dynamic behavior of a plug flow electrochemical reactor for a step change in flow rate. Ibrahim D S[14] investigated the performance of a plug flow electrochemical reactor with a cylindrical mesh electrode. The presence of a dead volume and short circuiting in the reactor decreased with an increase in the flow rate. The results obtained show the positive influence of the mesh electrode on the flow dynamic behavior. For a mesh plate electrode plug flow electrochemical reactor (MPE-PFER), Sato Kazuhiko[15] proposed a reactor with a similar structure but did not conduct in-depth research. Wang J[16] compared it with the traditional tubular electrochemical reactor, and the results showed that the turbulence intensity is clearly increased by 200% around the electrode surface.

The flow inside the electrocatalytic oxidation reactor is a gas-liquid two-phase flow. During the working process, the reactor generates gas on the surface of the electrode plate. Gas precipitates after nucleation to form a small bubble group. Wu W S[17] studied the effect of bubbles on the dispersion in the fluid close to the wall in a parallel plate electrochemical reactor. The results showed that the average residence time is almost unaffected by gas bubbles. Li Tingting[18] used CFD to study bubble behavior and believed that bubbles can enhance the degree of turbulence in the internal flow field. However, there are no effective experimental research results on bubble behavior under actual conditions.

Particle image velocimetry (PIV) is an emerging effective technique for measuring flow field conditions[19-22]. Flow field testing using PIV has become an effective method to study the motion of the flow field[23-27]. In the existing research results, hydrodynamics in a laboratory-scale VPERGE reactor – for three different current densities – was carried out[28]. The gas velocity field was obtained by using PIV. Measurement errors related to the use of this technique were discussed. A full flow field test of the MPE-PFER using PIV was proposed[29]. However, in these research results, only the single-phase flow field test was carried out, and the influence of the bubbles generated on the electrodes on the flow field under actual working conditions was not considered. There are few data on the flow field of the new type of plug flow electrochemical reactor with mesh plate electrodes, especially the flow field data of gas-liquid two-phase flow. We hope to obtain the flow characteristics of this kind of reactor to provide a reliable basis for future research.

Fluorescent tracer particles were used instead of polystyrene tracer particles, which could emit strong fluorescence under the excitation of a laser source and be captured by a high-speed camera to accurately reflect the flow of the liquid phase in a gas-liquid two-phase flow under bubble disturbance.

In this paper, particle image velocimetry technology (PIV) was used to test the flow field of an MPE-PFER under simulated working conditions, and the flow field data in the reactor under different working conditions were obtained. Flow field analysis was carried out, and based on the results of this analysis, the structure of the reactor was optimized to improve the processing capacity of the reactor.

2. MATERIALS AND METHODS

2.1. Experimental equipment

The experiment was carried out in a plug flow electrochemical reactor with a total length of 1 m and a longitudinal section length and width of 0.1 m, as shown in Fig. 1:

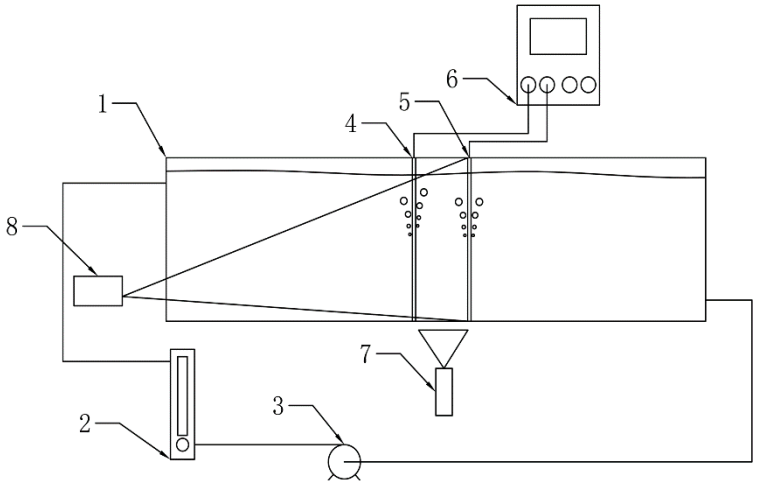

Figure 1. Schematic diagram of PIV experimental device: (1) Electrolytic cell, (2) Rotameter, (3) Pump, (4,5) Mesh plate electrode, (6) Power supply, (7) High-speed camera

The material is plexiglass with good light transmission, which is conducive to experimental observation. The electrocatalytic system consists of an electrode pair and a constant voltage/constant current DC power source. The electrode is a mesh electrode with a length of 0.1 m and a width of 0.1 m, as shown in Fig. 2. The opening ratio of the electrode was 0.25.

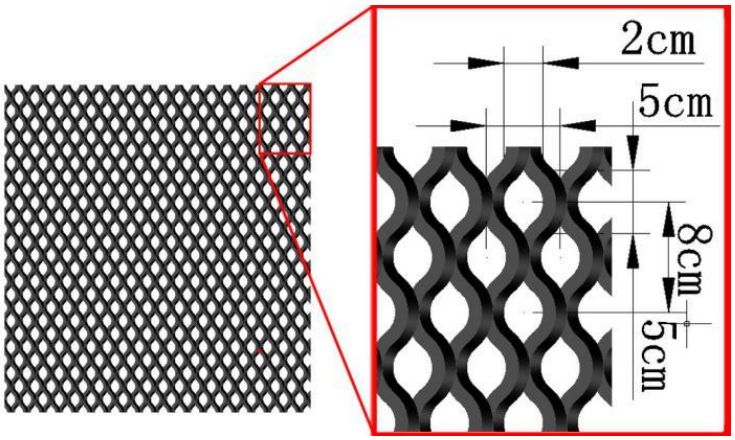

Figure 2. Mesh plate electrode structure

The electrodes are arranged in parallel in the vertical direction in the electrochemical reactor, and

the circulating flow rate is controlled by the rotameter. The data of the PIV test system devices are shown in Table 1. The liquid phase of the reactor is distilled water, which is filled with the reactor. Anhydrous sodium sulfate (0.3 mol) was added as a supporting electrolyte, and an appropriate amount of fluorescent tracer particles was distributed.

Table 1. PIV test system devices

Devices	Specification/model
Pulsed laser source	LPY700
High speed camera	4MX
Camera lenses	Nikon 50 mmf/1.8 D
PIV data processing system	Davis

2.2. Experimental setup

The devices are connected with silicone hoses, as shown in Fig. 1. The components of the test system are fully mixed and poured into the reactor. The mesh electrodes are positioned in parallel. The gap between the electrodes is 10 cm. The anode is made of titanium and coated with lead dioxide. The cathode material is titanium. The mesh electrodes are connected to the DC power supply to maintain the current at 1 A. The actual working condition is simulated by means of bubble generation in electrolytic water.

The presence of a jet at the inlet of the reactor will affect the experimental observation. To reduce the influence of the jet on the flow field, a jet baffle was made using transparent PVC and placed at the inlet of the reactor, as shown in Fig. 3.

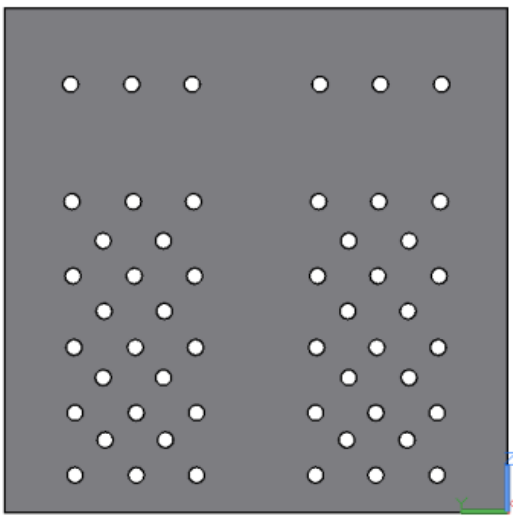

Figure 3. Jet baffle

The internal flow rate of the reactor was controlled by a rotameter, as shown in Table 2.

Table 2. Experimental flow rates

Rate of flow L/h	Reactor flow velocity m/s	Inlet flow velocity m/s
0	0	0
40	0.0011	0.1415
80	0.0022	0.2831
120	0.0033	0.4246

After the flow field is stabilized, the laser light source is used to illuminate the laser at different cross-section positions, and the cross-sectional position is as shown in Fig. 4.

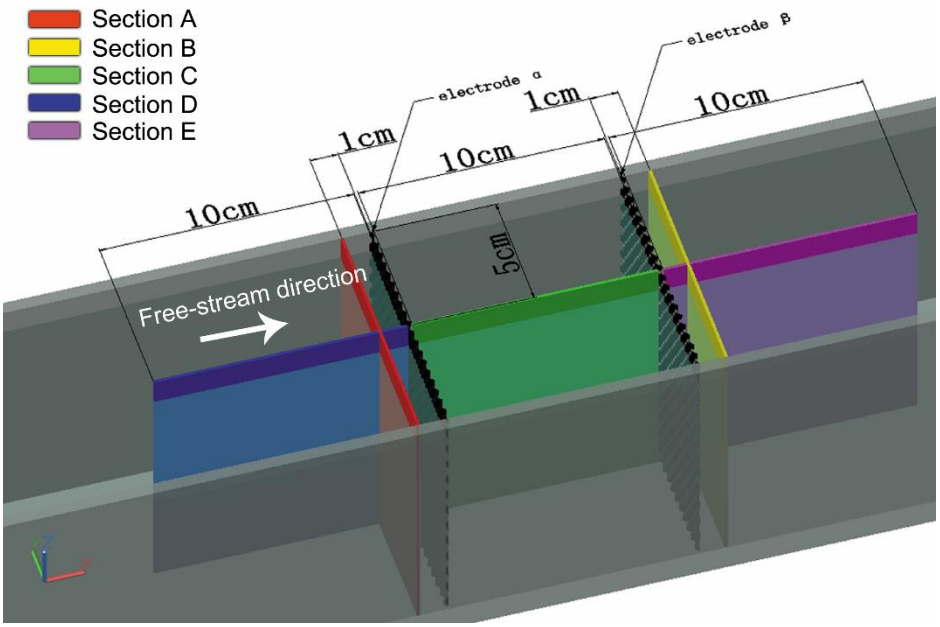

Figure 4. Section position diagram

The laser frequency is irradiated at 100 Hz, and the flow field image is recorded using a high-speed camera. The recording frequency of the camera is the same as the laser frequency. The recording time of each group of flow fields is 30 s, and the number of recorded pictures is 3,000. Using the Davis system, using the cross-correlation algorithm[30-31], the average flow field is calculated through 3,000 pictures during the recording time to obtain flow field data such as the velocity vector and the velocity contour.

2.3. Fitting formulas

When the fluid passed through the electrodes, energy loss occurred due to resistance. Due to the slow flow velocity, the influence of fluid viscous force was negligible. The energy loss of the fluid flowing from section A through the horizontal direction of section B can be expressed as[32]:

$$H_w = 2H_m + H_g + H_f = \frac{v_A^{\ 2} - v_B^{\ 2}}{2g} \quad (1)$$

The expressions in Eq. (1) are:

$$H_f = \lambda \frac{l u_1^{\ 2}}{2Rg} \quad (2)$$

$$H_m = \varepsilon \frac{u_2^{\ 2}}{2g} \quad (3)$$

According to the calculation in reference 33, the wall resistance coefficient of the open square groove is calculated as follows[33]:

$$\lambda = \frac{8}{2.5 \ln \frac{11 \cdot \frac{B}{2}}{\Delta} \cdot \frac{1.25}{r}} \quad (4)$$

B is the width of the reactor, which is 0.1 m. Δ is the wall roughness. *r* is the dimensionless width-depth ratio, and the expression is

$$r = \frac{2H}{B} \quad (5)$$

H is the reactor depth, which is 0.1 m. Substituting the above values into Eq. (4), the expression for λ is:

$$\lambda = \frac{8}{(2.5 \ln \frac{0.34375}{\Delta})^2} \quad (6)$$

For the plexiglass used in the reactor, Δ is 0.01 mm. The expression for *R* is:

$$R = \frac{A}{x} \quad (7)$$

A is 0.01 m^2, and *x* is 0.3 m. Φ is the opening ratio of the electrode. The expression for u_2 is:

$$u_2 = \frac{u_1}{\Phi} \quad (8)$$

3. RESULTS AND DISCUSSION

3.1. The effect of flow rate on the flow field

To investigate the effect of flow rate on the flow field in the reactor, the inlet side anode and the outlet side cathode had reactor flow velocities of 0.0011 m/s, 0.0022 m/s and 0.0033 m/s, respectively; the flow field velocity distribution was measured in different sections; and the velocity data at different positions in the flow field were obtained.

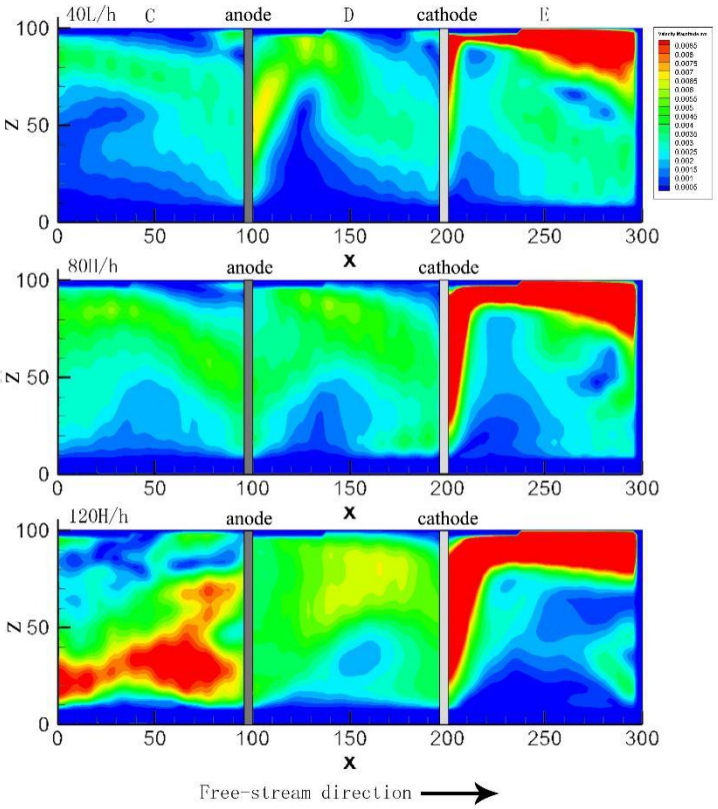

Figure 5. Longitudinal section velocity contours

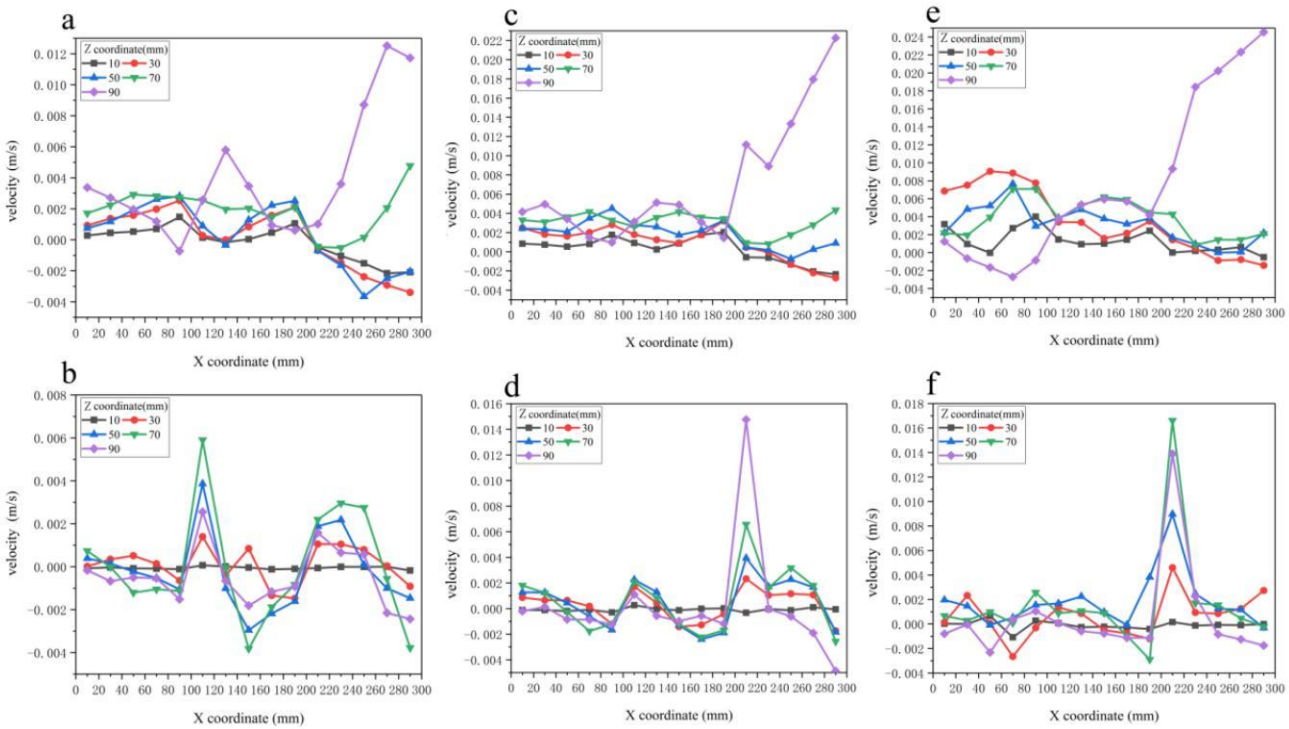

Figure 6. X-direction (a) and Z-direction (b) velocity at different positions under a flow velocity of 0.0011 m/s, X-direction (c) and Z-direction (d) velocity at different positions under a flow velocity of 0.0011 m/s, X-direction (e) and Z-direction (f) velocity at different positions under a flow velocity of 0.0033 m/s

As shown in Figs. 5, 6a, and 6c, at X-coordinates from 0-100 mm, before the liquid phase flowed through the electrode, the flow pattern was a plug flow. This finding was consistent with the results of the study on the flow of a single phase in MPE-PFER[16]. As shown in Fig. 6e, at the X-coordinate of 0-100 mm, the flow velocity was 0.0033 m/s, the baffle was insufficient to completely counteract the jet, the flow in front of the electrode was unstable, and a turbulent zone occurred. At the X-coordinate of 90-110 mm, where the liquid passed through the first electrode, the flow velocity in the X direction was reduced by 40%-60% due to the structure of the electrode and the blockage of the bubble group on the surface (Fig. 6e; Z-coordinate less than 90 mm). This finding was consistent with Shao's research[29] that the mesh electrode will block the axial flow and produce a certain backflow. Due to the escape of the bubble group, the surrounding liquid was moved, and the velocity in the Z direction was increased by approximately 0.002-0.003 m/s (Fig. 6e; Z-coordinate equal to 90 mm). As shown in Fig. 5, at the X-coordinate of 100-200 mm, as the flow velocity increased, the flow leading to this region changed from the eddy current caused by the bubble group to the plug flow. As shown in Fig. 5, at the X-coordinate of 200-250 mm (section E in Fig. 4), after passing through the second plate, the gas of the electrode surface was pushed by the liquid and escaped, and the bubble accumulated at the angle between the electrode and the upper liquid surface. As shown in Figs. 6a, 6c, and 6e, at the X-coordinates of 200-300 mm, the horizontal flow velocity of the upper layer was greatly increased, and the flow velocity difference was not large as in other regions. As shown in Figs. 6b, 6d, and 6f, at the X-coordinates of 200-240 mm, the velocity in the Z direction increased significantly near the plate. After flowing through approximately 20 mm, the velocity decreased and changed to the negative Z direction. After passing through the electrode, the upward escape of the bubble accumulated near the liquid level, so the liquid moving upward with the bubble produced different degrees of reflux, thus producing different degrees of velocity component along the negative direction of Z. Thereafter, the flow pattern was a plug flow with a relatively high upper flow velocity and a smooth lower flow velocity. With increasing velocity, the X direction velocity decreased as the electrode and bubbles blocked the flow. For the liquid in Fig. 6, after passing through the electrode, bubbles accumulated near the liquid level, so the liquid moving upward with the bubble produced different degrees of reflux, thus producing different degrees of velocity component along the negative direction of Z. Under the condition of a lower flow rate, as shown in Fig. 6b, the X-coordinate was 90-110 mm, and the Z direction velocity increasing effect of the first plate was more obvious. At higher flow rates, as shown in Figs. 6d and 6fb, the X-coordinates at 190-210 mm were more pronounced at the second electrode. Under low flow rate conditions, the horizontal driving force of the liquid phase was insufficient to dominate the flow. The flow field between the electrodes was mainly dominated by the escape of the bubble group. In general, due to the rising effect of the bubbles, eddies appear to different degrees behind the plates. Compared with the research results of Wang and others[16,18,29], the effect of bubbles on the flow field was very obvious, and the plates were not ideal single-phase columns. As for plug flow, different liquid layers had different flow rates, and the flow in the lower part of the reactor was relatively slow, so the generation and movement of bubbles should be considered in future research. As the flow velocity increased, the horizontal driving force exceeded that of the bubble group. The action caused the flow field in the reactor to be mainly a horizontal plug flow. When the flow velocity was higher, the flow in the reactor became more unstable. The increase in the flow rate was beneficial to accelerate the detachment and escape of the bubbles on

the electrode surface and alleviate the decrease in the effective reaction area caused by the bubbles adhering to the electrode surface. At the same time, the regeneration rate around the electrode was accelerated. Therefore, increasing the flow rate in an appropriate range was beneficial to the efficient development of electrocatalytic reactions.

3.2. Numerical analysis of energy loss between electrodes

To obtain the resistance coefficient ε of the new mesh electrode and the resistance loss H_g caused by the bubble group blocking effect, the values of v_A and v_B under different given flow rate conditions were obtained from the PIV test results, and when Eqs. (2-8) were substituted into Eq. (1), then Eq. (1) became:

$$\varepsilon \frac{u_2^{\ 2}}{g} + H_g = \frac{v_A^{\ 2} - v_B^{\ 2}}{2g} - \lambda \frac{l u_1^{\ 2}}{2Rg} = H_w - H_f \quad (9)$$

where ε and H_g were unknown, numerical fitting was performed, and the fitting formula was obtained. The results were as follows:

$$0.07024 \frac{u_2^{\ 2}}{g} + 1.74638 \times 10^{-7} = H_w - H_f \quad (10)$$

The R-squared was 0.96654. In this formula, u_1 was substituted for the theoretical value. The average flow velocity between the plates was obtained from the flow field distribution, as shown in Table 3:

Table 3. Theoretical and experimental flow velocities

Rate of flow L/h	Theoretical values m/s	Experimental values m/s
40	0.0011	0.001531
80	0.0022	0.002504
120	0.0033	0.003699

Substituting the experimental values into Eq. (9) and performing numerical fitting, the fitting formula is as follows:

$$0.0701 \frac{u_2^{\ 2}}{g} + 1.73646 \times 10^{-7} = H_w - H_f \quad (11)$$

The R-squared was 0.96656. Comparing the ε and H_g obtained by fitting Eq. (10) and Eq. (11), the deviations were 0.2% and 0.6%, respectively. It could be considered that the experimental value of u_1 was not much different from the theoretical values and could be used to substitute the theoretical values for fitting. Then, the experiment was carried out by changing the position of the electrodes, and the flow field data were measured for numerical fitting to obtain the fitting results:

Table 4. Fitting results under different conditions

Working condition	ε	Hg	R-squared
α electrode-anode	0.07024	1.74638E-7	0.96654
α electrode-cathode	0.07235	6.80636E-7	0.92289

The difference in the ε value obtained by the fitting was not large, the fitting result of the α electrode-anode condition was better than the cathode condition, and the R squared was the higher than the cathode condition. Therefore, the data under this condition are used for analysis.

As shown in Figs. 7 and 8, substituting u_1 values of 0.0001-0.008 m/s into Eq. (2) and Eq. (3), the histogram and percentage histogram of H_m, H_g and H_f at different velocities were obtained.

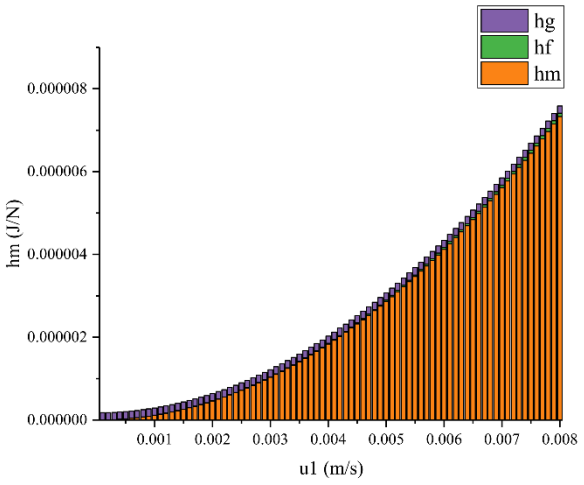

Figure 7. Energy loss histogram

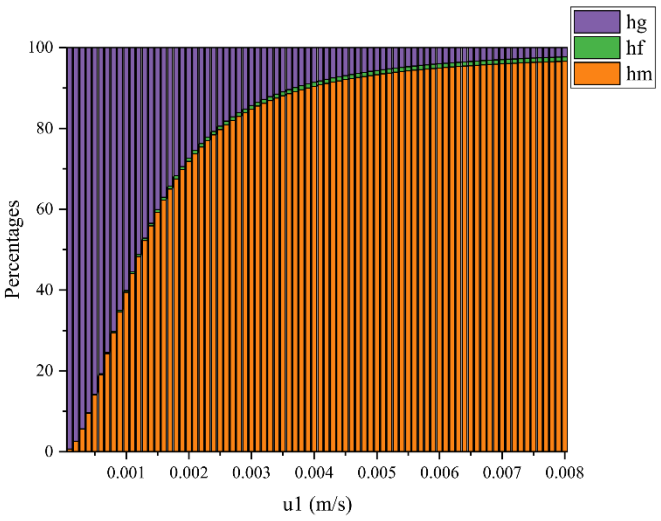

Figure 8. Energy loss percentage histogram

With increasing velocity, the main energy loss changed from H_g to H_m. Although H_f increased with velocity, it could be negligible compared with total energy loss. When u_1 was greater than 0.0013 m/s, the proportion of H_m exceeded H_g, indicating that at higher flow velocities, the energy loss between the reactor electrodes was mainly attributable to the resistance loss caused by the mesh plate electrodes. In Shao's research[29], the pressure drop at the outlet of the reactor increased with increasing flow rate. Consistent with the conclusion obtained in this section, the increase in the flow rate will increase the energy loss of the fluid. Under the same axial inlet mode and flow rate of 0.006-0.008 m/s, the pressure drop in the study increased by approximately 30%. In this study, the energy loss increased by approximately 60% because Shao's research did not consider the effect of bubbles on the flow and the kinetic energy loss of the fluid and only calculated the pressure drop, resulting in a small increase. In practical engineering applications, there were multiple sets of electrodes in the reactor. By changing the structure or arrangement of the electrodes to reduce the drag coefficient, the internal pressure drop of the reactor could be effectively reduced, the turbulence intensity could be enhanced, and the energy dissipation could be reduced.

3.3. The diversion effect of mesh holes

The normal direction of the mesh plane of the mesh electrode was not perpendicular to the liquid flow direction but had a certain angle, as shown in Fig. 9:

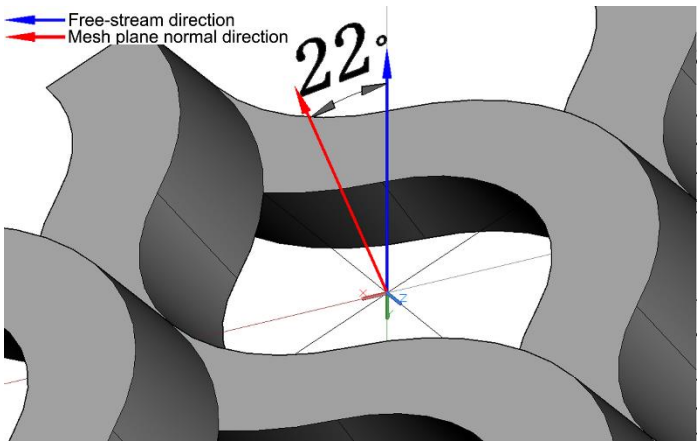

Figure 9. Mesh structure diagram

It was speculated that this geometry might produce a horizontal velocity component to the flow. Under the inlet-side anode and outlet-side cathode conditions, the velocity vector diagram of the parallel electrode cross-section was obtained according to different flow velocities and analyzed.

For the parallel section of the inlet side electrode, the liquid impinged on the electrode, forming a backflow that was disturbed by the bubbles on the surface of the plates. As shown in section A of Fig. 10, as the flow velocity increased, the electrode guided the liquid more effectively, and the horizontal velocity increased. For the parallel section of the outlet side electrode, the flow field was mainly

dominated by the bubble group escaping movement. The bubble group on the electrode surface moved with the flowing liquid phase, partially passed through the mesh hole, and then escaped to the liquid surface. A smooth, vertical upward flow was generated on the upper part of the electrode. As shown in section B of Fig. 10, the flow area became larger as the inlet flow rate increased. After the flow of the bubble group passed through the electrode, it was guided by the mesh of the electrode, and a velocity component in the horizontal direction was generated. As the flow rate increased, the magnitude of the velocity component increased, as shown in Fig. 11. This is different from the symmetrical velocity distribution results presented by the cross-section of parallel plates in Wang's and Li's research[16,18]. This was because their study simplifies the mesh structure in the mesh model and does not reflect whether the mesh structure actually has a diversion effect. Through observation, the special mesh structure of the mesh electrode used in this paper was consistent with the speculation, which confirmed the authenticity and reliability of the PIV experimental results.

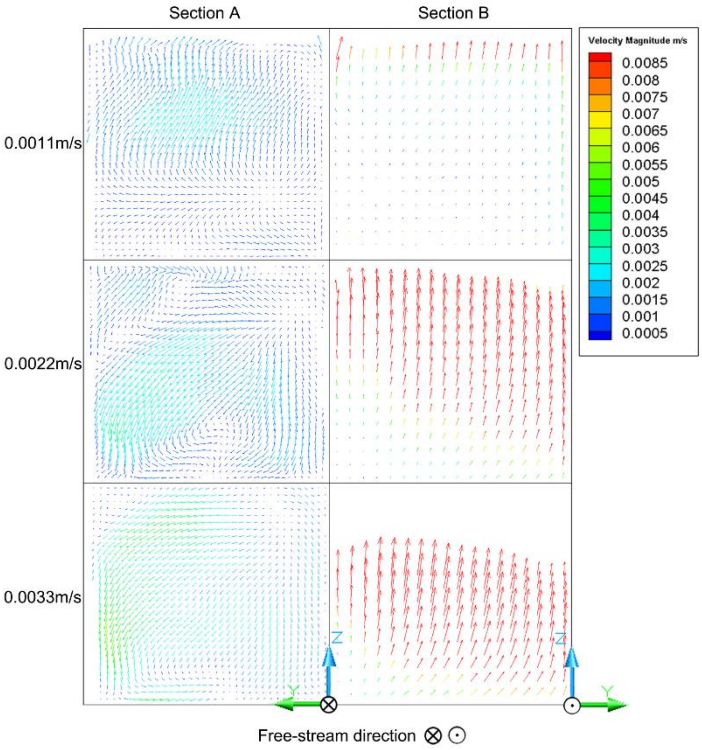

Figure 10. A section and B section velocity vectors

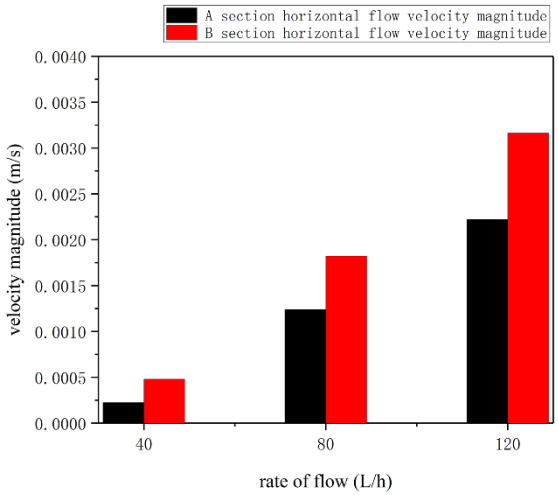

Figure 11. A section and B section horizontal flow velocity magnitude

The results show that the unique structure of the electrode had a diversion effect on the liquid flow. In practical engineering applications, this horizontal guiding effect could be utilized to change the internal flow field shape of the reactor, design the flow channel, increase the average residence time, and improve the performance of the reactor.

3.4. The effect of bubble behavior on the flow field

In the existing research results[34-36], the influence of bubbles on the flow field and mass transfer performance in the reactor cannot be ignored. During the working process of the MPE-PFER, the bubbles generated on the surface of the electrode would disturb the flow field in the reactor, as shown in Fig. 12.

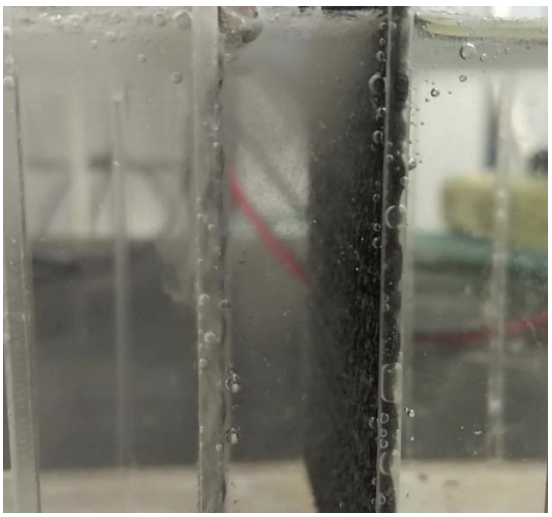

Figure 12. Bubble distribution in the reactor under a flow rate of 80 L/h

To study the effect of bubble behavior on the internal flow field, the following investigation was

carried out.

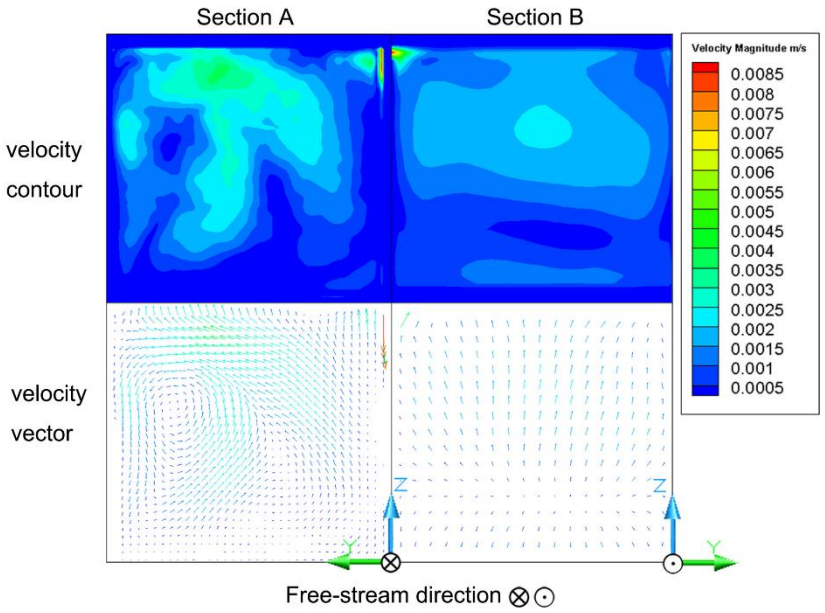

Figure 13. A section and B section flow field without horizontal flow

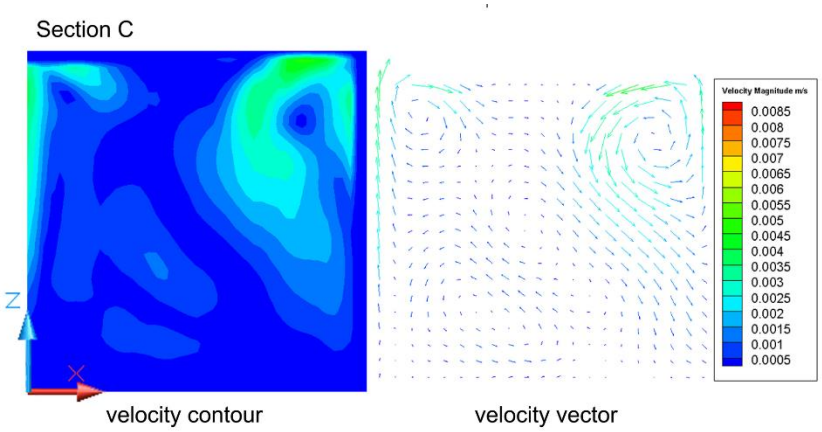

Figure 14. C section flow field without horizontal flow

The results showed that when there was no liquid phase flow, the bubbles generated on the surface of the electrodes continuously gathered on the plates, precipitated, and moved vertically upward under the action of buoyancy. A large number of bubbles formed a group of bubbles, which disturbed the liquid phase around the surface of the electrode and drove the liquid phase to move vertically upward. The bubbles were mainly generated at 2/3 of the upper electrode, and bubbles at the lower portion of the plates were hardly generated. This was consistent with the conclusion of Hreiz's research in 2015[28], as shown in Figure 1 of his research article.

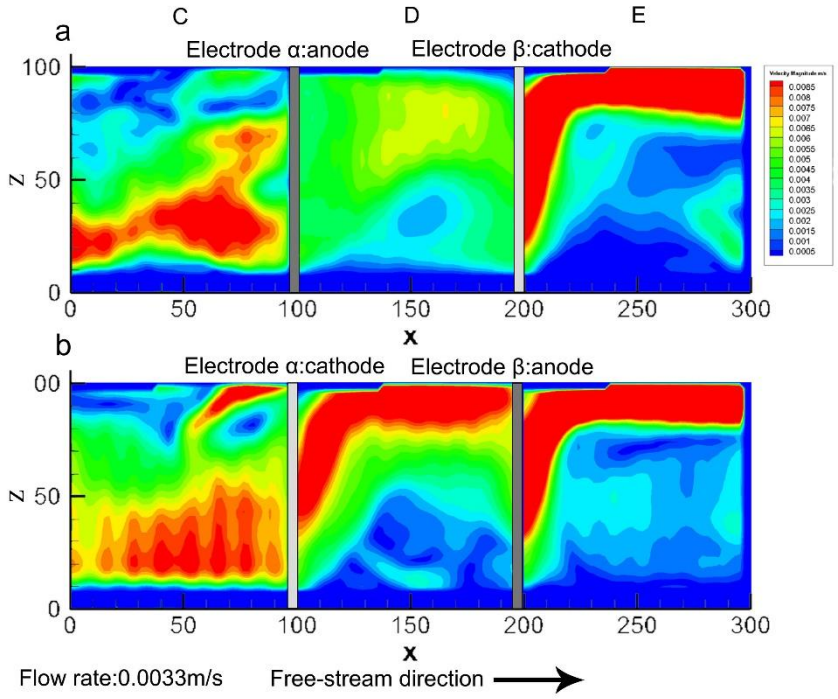

Figure 15. Longitudinal section velocity contours under different electrodes placed

As shown in Fig. 13, for the A section anode, bubbles were mainly generated between the electrodes, and some bubbles passed through the mesh electrode and were guided by the horizontal direction of the mesh to generate a vortex on the inlet side. For the B section cathode, the amount of bubble generation was large, and the escape of the bubble exceeded the guide effect of the mesh. Approximately 2/3 of the upper plate supported a stable vertical upward flow, and the lower part was the flow stagnation area.

As shown in Fig. 14, as the amount of bubbles increased, the bubbles accumulated at the angle between the electrode surface and the upper liquid surface and moved in the direction away from the electrode at the liquid level. Bubbles were generated in both electrodes, and the two streams at the liquid level collided with each other. Therefore, a vortex was formed on the upper surface of the electrodes. The amount of cathode gas (hydrogen) generated by electrolysis of water was twice that of the anode (oxygen), so the vortex velocity at the cathode was higher than at the anode.

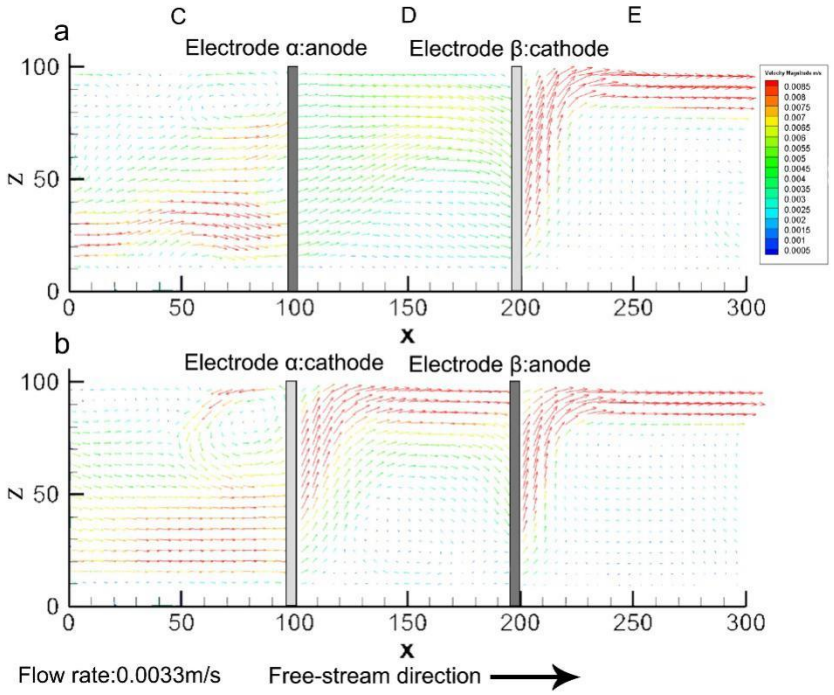

Figure 16. Longitudinal section velocity vectors under different placed electrodes

When the reactor was under actual conditions, as shown in section E of Fig. 15, the liquid flow with bubbles flowed horizontally and acted together with buoyancy to make the bubbles flow diagonally upward. As shown in Fig. 16, at the X-coordinate of 200-240 mm, the vortex between the plates disappeared, and bubbles finally accumulated on the liquid surface, resulting in a higher horizontal velocity of the upper part of the liquid. When the amount of bubble production increased, as shown in Fig. 15b, the inlet side was the cathode, and the bubble layer on the surface of the plate was thicker, which had an obvious blocking effect on the liquid flow. This was consistent with the conclusion of Cavalcanti[37] that bubble film is generated on the surface of the plate as the speed of the upper part of the reactor increased, and the same conclusion was reached in similar studies conducted by Mandroyan[38] and Qureshy[39]. The horizontal liquid flow drove the bubbles away from the electrode surface, which increased the effective plate area and facilitated the efficient electrochemical reaction. This phenomenon has been described in detail in the study of Eigeldinger[40]. The flow pattern after passing through one electrode was consistent with that of the two electrodes in Fig. 15a. It could be confirmed that when the generated amount of bubbles was larger, the flow field between the electrodes was more likely to be stable and consistent.

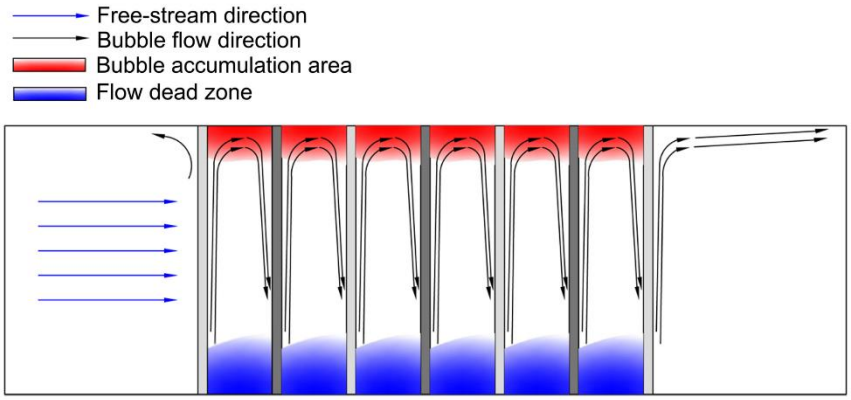

Figure 17. Schematic diagram of the general flow of the reactor

According to the above analysis, the flow field between the electrodes was formed by the horizontal plunger flow, the bubble group escaping from the electrode surfaces, and the joint influence of the electrodes and the bubble group on the axial flow barrier. The general rule of the flow field between plates is shown in Fig. 17. The upper part of the space between the electrodes was the bubble accumulation area, and the lower part was the dead flow area. The bubble drove the liquid phase to flow in an inverted U shape between the electrodes. Under stable working conditions, a characteristic flow field between the electrodes was formed. In the reactor optimization process, the structure optimization could be carried out to eliminate the upper bubbles and utilize the lower dead zone between the electrodes to improve the reactor efficiency.

4. CONCLUSIONS

Flow fields at different positions inside the MPE-PFER with bubble escape conditions were analyzed. The results showed that the reactor flow velocity was the most important factor affecting the internal flow of the reactor. The increase in the flow velocity was beneficial to drive the bubbles on the surface of the electrodes to escape faster, reduce the eddy current generated by the bubble movement, and make the dominant flow a horizontal plug flow, thus enhancing the internal turbulence and the mass transfer. The reactor structure affected the internal flow pattern of the reactor. The energy loss caused by the grid plate electrode structure accounted for the main part of the total energy dissipation under the actual condition of a higher flow rate. The particularity of the mesh electrode structure changed the flow state through the electrodes, and the horizontal guide effect could be used to design different electrode arrangements. The generation and escape of bubbles are important factors. The upward movement of buoyancy drove the surrounding liquid to move and eventually accumulate on the liquid surface. Under this influence, the general rule of reactor flow was as follows: smooth plunger flow in front of the plate, inverted u-shaped flow between the electrodes, a bubble accumulation area in the upper part, a dead flow area in the lower part, plunger flow in the back of the plate, and fast flow velocity in the upper part. The performance of the MPE-PFER should be optimized by eliminating the dead flow zone at the bottom of

the reactor, increasing the average residence time by designing a flow passage with net plate conductivity, and optimizing the structure to accelerate bubble detachment.

References

1. A. Anglada, A. Urtiaga and I. Ortiz, *J. Chem. Technol. Biotechnol.*, 84 (2009) 1747-1755.
2. S. Garcia-Segura and E. Brillas, *J. Photochem. Photobiol., C.*, 31 (2017) 1-35.
3. C. Carlesi, N. Guajardo Ramírez, D. Carvajal, M. Cataldo Hernández and D. Fino, *Desalin. Water Treatatment*, 54 (2015) 1556-1562.
4. M. Govindaraj, R. Rathinam, C. Sukumar, M. Uthayasankar and S. Pattabhi, *Environ. Technol.*, 34 (2013) 503-511.
5. X. Ma, Y. Gao, Y. Cui, H. Huang and J. Han, *Desalin. Water Treatment*, 57 (2016) 19557-19565.
6. K. Scott, *J. Appl. Electrochem.*, 19 (1989) 531-534.
7. S. König, M. R. Suriyah, T. Leibfried, *J. Power Sources*, 360 (2017) 221-231.
8. S. A. Martínez-Delgadillo, M. A. Gutiérrez, I. D. Barceló and J. M. Méndez, *Comput. Chem. Eng.*, 34 (2010) 491-499.
9. U. M. López-García, P. E. Hidalgo, J. C. Olvera, F. Castañeda, H. Ruiz and G. Orozco, *Fuel*, 110 (2013) 162-170.
10. A. N. Colli and J. M. Bisang, *Electrochim. Acta*, 56 (2011) 7312-7318.
11. G. Rodríguez, F. Z. Sierra-Espinosa, J. Teloxa, A. Álvarez and J. A. Hernández, *Desalin. Water Treatment*, 57 (2016) 22968-22979.
12. F. C. Walsh and C. P. de Leon, *Electrochim. Acta*, 280 (2018) 121-148.
13. J. M. Bisang, *J. Appl. Electrochem.*, 31 (2001) 403-409.
14. D. S. Ibrahim, C. Veerabahu, R. Palani, S. Devi and N. Balasubramanian, *Comput. Fluids.*, 73 (2013) 97-103.
15. K. Sato, K. Terakazaki, T. Uchihori, *JP198178679*, (1979) 12-03.
16. J. Wang, T. Li, M. Zhou, X. Li and J. Yu, *Electrochim. Acta*, 173 (2015) 698-704.
17. W. S. Wu, G. P. Rangaiah and M. Fleischmann, *J. Appl. Electrochem.*, 23 (1993) 113-119.
18. T. Li, X. Li, F. Chen and J. Wang, *J. Electrochem. Soc.*, 161 (2014) E81-E86.
19. R. D. Keane and R. J. Adrian, *Appl. Sci. Res.*, 49 (1992) 191-215.
20. C. D. Meinhart, S. T. Wereley and J. G. Santiago, *Exp. Fluids*, 27 (1999) 414-419.
21. C. E. Willert and M. Gharib, *Exp. Fluids*, 10 (1991) 181-193.
22. R. J. Adrian, *Exp. Fluids.*, 39 (2005) 159-169.
23. J. Westerweel, *Meas. Sci. Technol.*, 8 (1997) 1379.
24. S. Burgmann, C. Brücker and W. Schröder, *Exp. Fluids*, 41 (2006) 319-326.
25. M. Lang, U. Rist and S. Wagner, *Exp. Fluids*, 36 (2004) 43-52.
26. D. Funfschilling and H. Z. Li, *Chem. Eng. Sci.*, 56 (2001) 1137-1141.
27. S. Besbes, I. Gorrab, M. ElHajem, H. Ben Aissia and J. Y. Champagne, *Part. Sci. Technol.*, (2019) 1-10.
28. R. Hreiz, L. Abdelouahed, D. Fuenfschilling and F. Lapicque, *Chem. Eng. Sci.*, 134 (2015) 138-152.
29. B. Shao, X. Li, T. LI, J. Wang, *Journal Of Zhejiang University (Engineering Science)*, 49 (2018) 130-135.
30. W. Cheng, Y. Murai, T. Sasaki and F. Yamamoto, *Flow Meas. Instrum.*, 16 (2005) 35-46.
31. B. Lecordier, M. Mouqallid, S. Vottier, E. Rouland, D. Allano and M. Trinite, *Exp. Fluids.*, 17 (1994) 205-208.
32. W. Jiang, Principles of chemical engineering, Tsinghua university press co. LTD, (2003), China.
33. Y. Yang, *Hydro-Science and Engineering*, 3 (1984) 59-69.

34. A. H. Essadki, B. Gourich, C. Vial and H. Delmas, *Chem. Eng. Sci.*, 66 (2011) 3125-3132.
35. T. Nierhaus, D. V. Abeele and H. Deconinck, *Int. J. Heat Fluid Flow.*, 28 (2007) 542-551.
36. M. A. Petersen and K. F. Reardon, *AlChE J.*, 55 (2009) 2468-2476.
37. R. D. S. Cavalcanti, S. R. D. Farias Neto and E. O. Vilar, *Brazilian Archives of Biology and Technology*, 48 (2005) 219-229.
38. A. Mandroyan, M. L. Doche, J. Y. Hihn, R. Viennet, Y. Bailly and L. Simonin, *Ultrason. Sonochem.*, 16 (2009) 97-104.
39. A. M. Qureshy, M. Ahmed and I. Dincer, *Int. J. Hydrogen Energy*, 41 (2016) 8020-8031.
40. J. Eigeldinger and H. Vogt, *Electrochim. Acta*, 45 (2000) 4449-4456.